All-optical tunable on-chip plasmon-induced transparency based on two surface-plasmon-polaritons absorption

Zhen Chai, Xiaoyong Hu, Hong Yang, and Qihuang Gong

Citation: Applied Physics Letters **108**, 151104 (2016); doi: 10.1063/1.4946763
View online: http://dx.doi.org/10.1063/1.4946763
View Table of Contents: http://scitation.aip.org/content/aip/journal/apl/108/15?ver=pdfcov
Published by the AIP Publishing

All-optical tunable on-chip plasmon-induced transparency based on two surface-plasmon-polaritons absorption

Zhen Chai,[1] Xiaoyong Hu,[1,2,a)] Hong Yang,[1] and Qihuang Gong[1,2]
[1]*State Key Laboratory for Mesoscopic Physics & Department of Physics, Collaborative Innovation Center of Quantum Matter, Peking University, Beijing 100871, People's Republic of China*
[2]*Collaborative Innovation Center of Extreme Optics, Shanxi University, Taiyuan 030006, People's Republic of China*

(Received 17 February 2016; accepted 1 April 2016; published online 12 April 2016)

All-optical tunable on-chip plasmon-induced transparency is realized in integrated plasmonic circuits based on two surface-plasmon-polaritons absorption induced polymerization of SU-8 photoresist. Owing to the enhanced interaction between surface plasmon polaritons and SU-8 guaranteed by the slow light effect around the transparency window and the strong light confinement effect of the plasmonic nanocavity modes, a continuous shift range of 24 nm in the central wavelength of the transparency window was obtained. The threshold power of the two surface-plasmon-polaritons absorption induced polymerization of SU-8 was as low as 100 μW, which is three orders of magnitude less than previous reports. *Published by AIP Publishing*. [http://dx.doi.org/10.1063/1.4946763]

Plasmon-induced transparency (PIT) originates from the strong destructive interference coupling between the wide-band superradiant plasmonic mode and narrow-band subradiant plasmonic mode.[1,2] Because of the slow light effect in the transparency window and strong localized field enhancement effect provided by plasmonic modes, PIT has great potential applications in the field of integrated photonic devices.[3,4] Recently, various plasmonic microstructures have been proposed to demonstrate PIT, such as metamaterials,[5–7] plasmonic crystals,[8–10] and metallic nanograting coupled with dielectric waveguides.[11–13] While only the on-chip PIT could be used in the chip-integrated photonic devices.[14–18] The basic realization method of on-chip PIT is based on the configuration of plasmonic nanocavities side-coupled a bus pasmonic waveguide.[14–18] Most of the plasmonic nanocavities are fabricated by using the microfabrication technology, such as the electron beam lithography (EBL) or focused ion beam (FIB) etching techniques.[19] However, limited by the microfabrication etching precision (10 nm for FIB etching system and 30 nm for EBL etching system), it is very difficult to ensure that structural parameters of fabricated samples are the same ones as the designed ones.[14–19] So, in general, there is a disparity between the measured results and the theoretically predicted ones.[20] The traditional resolution is to fabricate several samples with the same structural parameters and select the best one to perform the optical measurement.[21] But, this method is passive and wastes many resources and time. Up to now, it is still a great challenge to realize a convenient and efficient post-processing of plasmonic nanocavities to achieve the satisfactory on-chip PIT.

Here, we report an approach to realizing the convenient and efficient post-processing of the plasmonic nanocavities based on two surface-plasmon-polaritons (SPPs) absorption induced polymerization of a negative tone photoresist bis(2-(oxiran-2-ylmethoxy)-3-(2-(oxiran-2-ylmethoxy)-5-(2-(4-(oxiran-2-ylmethoxy)phenyl)propan-2-yl)benzyl)-5-(2-(4-(oxiran-2-ylmethoxy)phenyl)propan-2-yl)phenyl)methane (SU-8), which ensures an all-optical and permanent tuning of on-chip PIT. The on-chip PIT was formed in a plasmonic microstructure composed of a plasmonic waveguide side-coupled two plasmonic nanocavities covered by a SU-8 photoresist layer in integrated plasmonic circuits. A transmission peak was formed in the transmission forbidden-band, realized based on destructive interference between two excitation pathways (directly exciting the superradiant microcavity mode and exciting the subradiant microcavity mode through the superradiant microcavity mode). The two SPPs absorption induced polymerization of SU-8 photoresist results in the increase of the refractive index of SU-8, which make the plasmonic nanocavity modes shift in the long-wavelength direction. Accordingly, the central wavelength of the transparency window shifts in the long direction. Owing to the enhanced interaction between SPPs and SU-8 photoresist guaranteed by the slow light effect around the transparency window and the strong light confinement effect provided by the plasmonic nanocavity modes, the total shift magnitude of the central wavelength of the transparency window reached 24 nm. The threshold power of the two SPPs absorption induced polymerization of SU-8 was as low as 100 μW, which is three orders of magnitude less than previous reports.[22,23]

The plasmonic microstructure sample without the SU-8 cover layer (Fig. 1(a)) consisted of a plasmonic waveguide side-coupled with two plasmonic nanocavities etched in a 300-nm-thick gold film deposited on SiO_2 substrate. Two nanogrooves formed the two plasmonic nanocavities. The length, width, and depth were 380, 150, and 150 nm for the horizontal nanocavity, and 270, 150, and 150 nm for the vertical nanocavity. The distance between the horizontal and vertical nanocavities was 20 nm in the vertical direction. Both of the horizontal and vertical nanocavities were centrosymmetric along the perpendicular bisector line of the horizontal nanogroove. The width and depth were 150 and 150 nm for the plasmonic waveguide. To effectively excite and collect the needed SPP modes, we fabricated a 300-nm-thick input-coupling grating (Fig. 1(b)) connecting with a 150-nm-deep triangular air nanogroove in the input port of

a)Author to whom correspondence should be addressed. Electronic mail: xiaoyonghu@pku.edu.cn

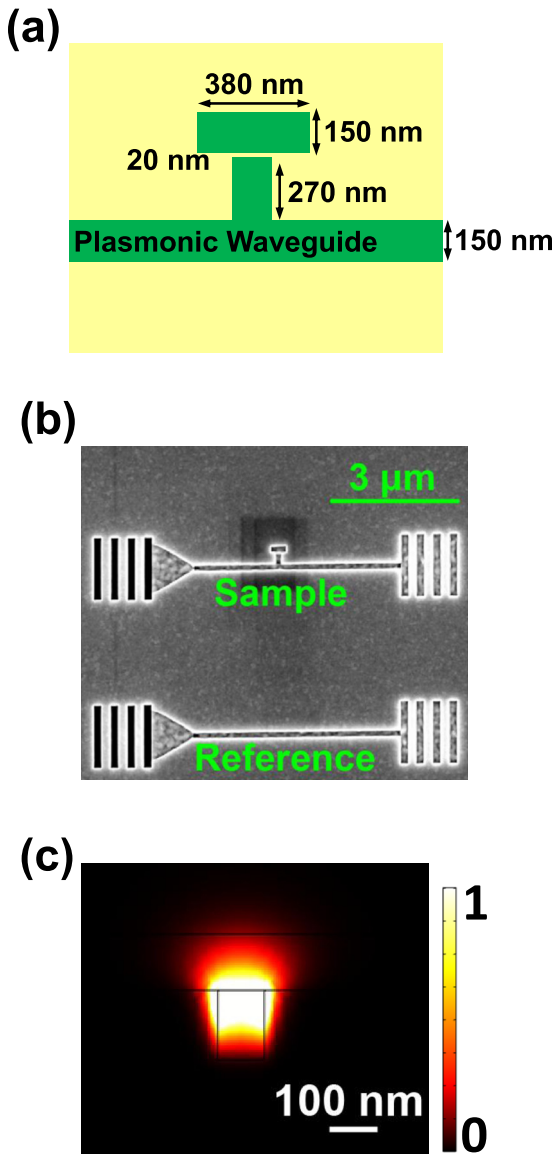

FIG. 1. Top view schematic structure (a) and SEM image (b) of the plasmonic waveguide side-coupled two plasmonic nanocavities, without the SU-8 cover layer. The length, width, and depth were 380, 150, and 150 nm for the horizontal nanocavity, and 270, 150, and 150 nm for the vertical nanocavity. (c) Calculated power density profile of the guided SPP mode in the plasmonic waveguide covered with the 120-nm-thick SU-8 cover layer under a CW incident light with the wavelength of 790 nm.

the plasmonic waveguide. A 150-nm-thick decoupling grating was etched in the output port of the plasmonic waveguide. We calculated the energy distributions (Fig. 1(c)) of the guided SPP mode excited by a 790-nm continuous wave (CW) incident light by using the finite element method (using a commercial software COMSOL Multiphysics).[14,15] The guided SPP modes were mainly located in the top port of the slot region of the plasmonic waveguide and extended into the upper SU-8 cover layer. This indicates that the plasmonic nanocavity modes are very sensitive to the refractive index change of the SU-8 cover layer.

The 300-nm-thick gold film was fabricated by using a laser molecular beam epitaxy growth system (Model LMBE 450, SKY Company, China), as detailed in Ref. 4. A focused ion beam etching system (Model Helios NanoLab 600, FEI Company, USA) was used to prepare the patterns of the plasmonic microstructures. Then, the spin coating method was used to fabricate the 120-nm-thick SU-8 (Gersteltec GM 1010, Switzerland) cover layer on the surface of plasmonic microstructures.

In order to study the on-chip PIT, we measured the linear transmission spectrum (Fig. 2(a)) of the plasmonic microstructure sample having the SU-8 cover layer by using a micro-spectroscopy measurement system.[14,18] The linear transmission was normalized with respect to the reference plasmonic waveguide with the same geometrical parameters. Limited by the tunable wavelength range of the Ti:sapphire laser system, we only measure the linear transmission spectrum from 700 to 1000 nm. A transmission peak appeared in the transmission forbidden-band, which indicates the formation of PIT. The central wavelength and peak transmission of the transparency window were 770 nm and 75%, respectively, which are in agreement with the calculated ones (Fig. 2(b)) by using the finite element method. We calculated the magnetic-field distribution of the plasmonic microstructure sample excited by the CW incident light with a wavelength of 750 nm (located in the transmission minimum in the short-wavelength direction), 770 nm (located in the transparency window center), and 820 nm (located in the transmission minimum in the long-wavelength direction) by using the finite element method. For the CW incident light at wavelength of 750 nm (or 820 nm), the magnetic-field distribution was mainly situated in the horizontal (or vertical) plasmonic nanocavity, and no SPP modes can propagate through the plasmonic waveguide, as shown in Fig. 2(c) (or Fig. 2(e)). For the 770-nm incident CW light, the magnetic field distribution (Fig. 2(d)) was mainly confined in both of the vertical and horizontal nanocavities, and the SPP mode can propagate through the plasmonic waveguide. The vertical nanocavity modes can be directly excited by the SPPs propagating in the plasmonic waveguide, which forms the superradiant modes. The horizontal nanocavity modes, only excited by the neighboring vertical nanocavity modes, construct the subradiant modes. Therefore, it is the destructive interference between the two excitation pathways (directly exciting the superradiant mode and exciting the subradiant mode through the superradiant mode) that forms the transparency window. According to our calculations by using the finite element method, the total radiation loss was 6.1% when the waveguide mode was incident on the plasmonic nanocavities for the 770-nm incident light. We calculated the linear transmission spectrum (Fig. 2(f)) of the plasmonic waveguide side coupled a single vertical (or horizontal) nanocavity with the same geometric parameters as above, covered by the SU-8 layer. The distance between the horizontal nanocavity and the plasmonic waveguide was set to be 20 nm. The central wavelength of the transmission valley was 770 nm for both the vertical and horizontal nanocavities, which responds to the resonant wavelength of individual plasmonic nanocavities. According to our calculations by using the finite element method, the resonance wavelength was 764 nm for the isolated horizontal plasmonic nanocavity and 766 nm for the isolated vertical plasmonic nanocavity.

To study the all-optical tunability, we measured the transmission changes (Fig. 3(a)) of the 750-nm signal laser as a function of the incident power by using the micro-spectroscopy

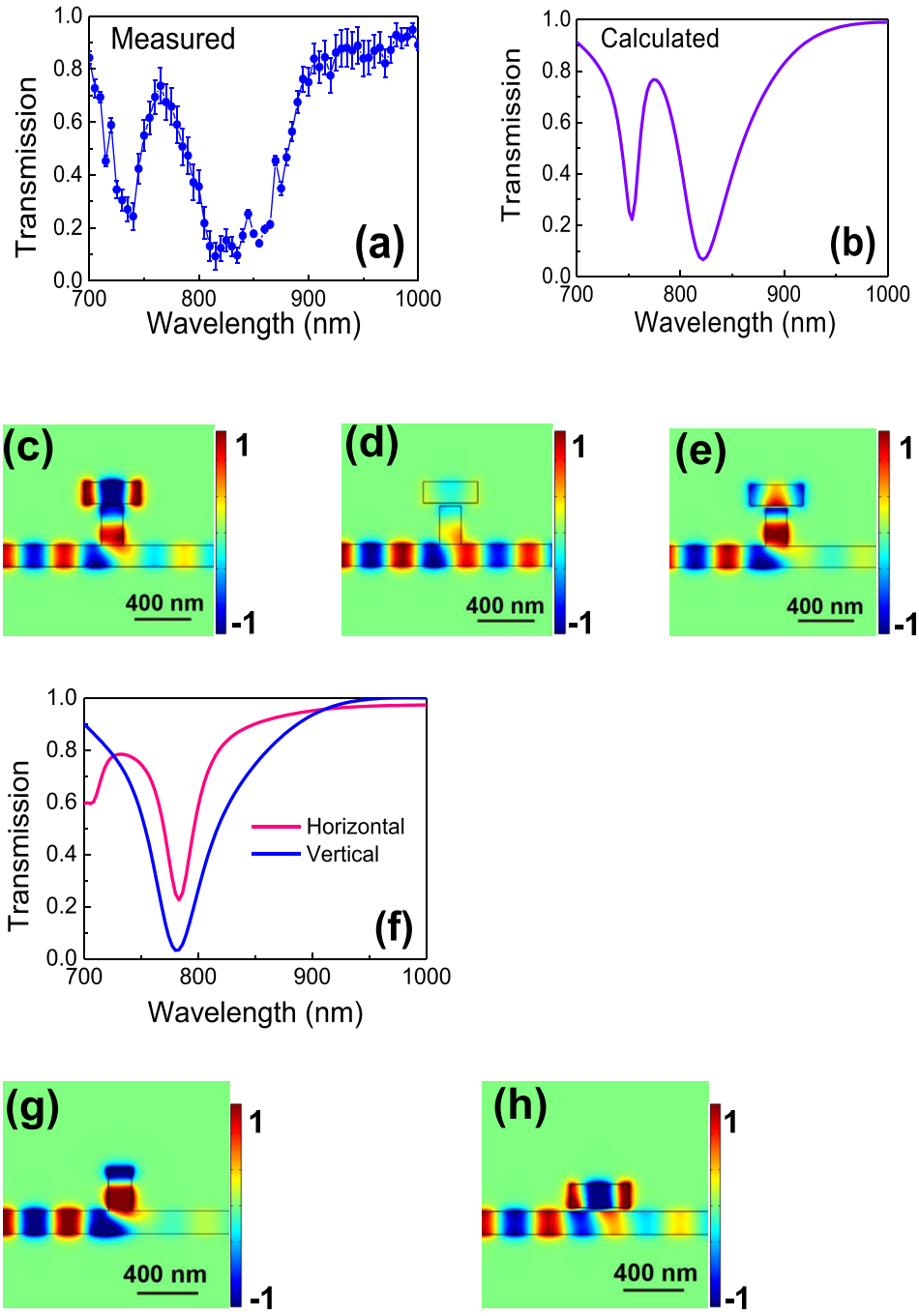

FIG. 2. Measured (a) and calculated (b) linear transmission spectrum of the plasmonic waveguide side-coupled two plasmonic nanocavities having the SU-8 cover layer. Calculated magnetic-field distributions of the plasmonic waveguide side-coupled two plasmonic nanocavities having the SU-8 cover layer under the excitation of a CW incident light with the wavelength of 750 nm (c), 770 nm (d), and 820 nm (e). (f) Calculated transmission spectrum of the plasmonic waveguide side-coupled the vertical (or horizontal) plasmonic nanocavity. Calculated magnetic field distribution of the plasmonic waveguide side-coupled the vertical (g) and horizontal (h) plasmonic nanocavities.

measurement system. A 120-fs, 76-MHz beam output from a Ti:Sapphire laser (model Mira 900F, Coherent Company, USA) was used as the light source. A chopper was used to reduce the repetition rate of the laser beam to 635 Hz in order to remove the influences of thermal effect. The wavelength of 750-nm dropped in the transmission minimum in the short-wavelength direction. When the incident power increased from 5 to 95 μW, the transmission of the signal light maintained the value of 25%. When the incident power was larger than 100 μW, the transmission of signal light increased. Deubel *et al*. and Shir *et al*. have pointed out that SU-8 photoresist could only be polymerized by a light whose photon energy was larger than 3.098 eV (corresponding to the photon wavelength of less than 400 nm), and two-photon absorption effect could be adopted to trigger the polymerization of the SU-8 photoresist by using an 800-nm, 120-fs laser beam.[24,25] Cumpston *et al*. and Thiel *et al*. also pointed out that the two-photon absorption probability depended quadratically on the laser intensity, which ensures the remarkable feature of a threshold power needed to trigger the two-photon-initiated polymerization of SU-8 photoresist.[26,27] Berini and Leon and Archambault *et al*. have noted that SPPs could be quantized and treated as quantum in term of energy, and it was possible to realize the nonlinear optical effect and process associated with two SPPs absorption.[28,29] The two SPPs absorption induced polymerization of SU-8 photoresist, accompanied with a increase in the refractive index of SU-8, has been confirmed by the measurement of Li *et al*.,[22,23] which results in a red-shift in the resonant wavelength of the plasmonic nanocavity modes. Accordingly, the central wavelength of the transparency window shifts in the long-wavelength direction, and the transmission of the 750-nm incident light increase.

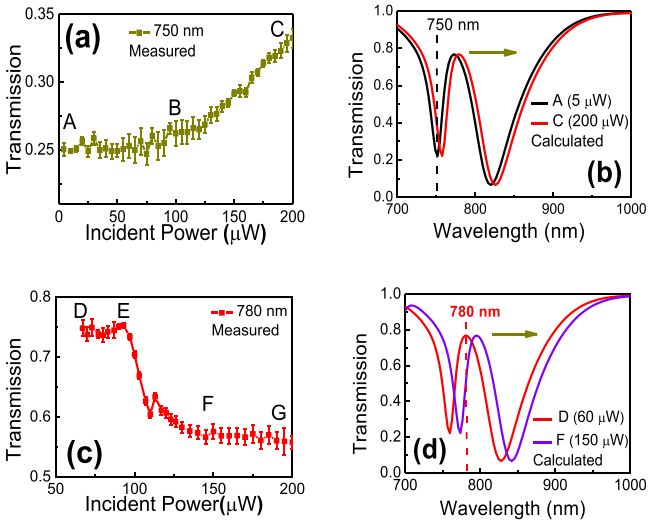

FIG. 3. (a) Measured transmission changes of the 750-nm signal light propagating through the plasmonic waveguide side-coupled two plasmonic nanocavities having the SU-8 cover layer as a function of incident power. (b) Calculated linear transmission spectrum of the plasmonic waveguide side-coupled two plasmonic nanocavities having the SU-8 cover layer with different incident power of 750-nm light. Arrow indicates the shift direction of the transparency window. (c) Measured transmission changes of the 780-nm signal light propagating through the plasmonic waveguide side-coupled two plasmonic nanocavities having the SU-8 cover layer as a function of incident power. (d) Calculated linear transmission spectrum of the plasmonic waveguide side-coupled two plasmonic nanocavities having the SU-8 cover layer with different incident power of 780-nm light. Arrow indicates the shift direction of the transparency window.

When the incident power was increased to 200 μW, the transmission of the 750-nm incident light increased to 34%. A threshold power of 100 μW was obtained for the two SPPs absorption induced polymerization of SU-8 photoresist, which was reduced by three orders of magnitude compared with previous reports.[22,23] The reason can be understood as following: first, the strong confinement of light into the subwavelength scale provided by plasmonic nanocavity modes enhances the interaction between SPPs and SU-8 photoresist. Second, the strong slow light effect was obtained around the transparency window of PIT, as shown in Fig. 4. We calculated the linear transmission spectrum (Fig. 3(b)) of the plasmonic waveguide side-coupled two plasmonic nanocavities having the SU-8 cover layer with different incident power of 750-nm light by using the finite element method. It is clear

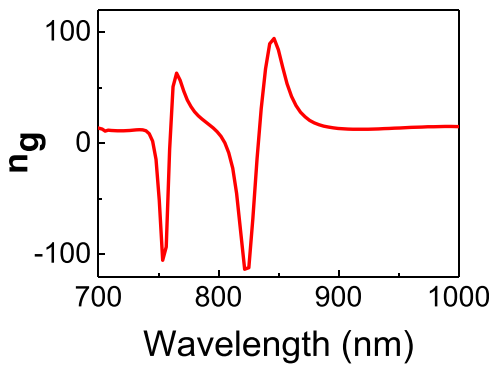

FIG. 4. Calculated group refractive index as a function of incident light wavelength for the plasmonic waveguide side-coupled two plasmonic nanocavities having the SU-8 cover layer.

that with when the incident power increased from 5 to 200 μW, the central wavelength of the transparency window changed from 770 to 780 nm, i.e., a 10 nm shift in the long wavelength direction was obtained. Accordingly, the transmission of the 750-nm light increased from 25% (at the incident power of 5 μW) to 34% (at the incident power of 200 μW). According to the coupled mode theory, the coupled mode equation used in our simulations can be expressed as[30]

$$T = 1 - \frac{1}{1 + [\omega - \omega_1 - |\kappa_2|^2/(\omega - \omega_2)]^2/\kappa_1}, \quad (1)$$

where ω_1 and ω_2 are resonance frequencies of the vertical and horizontal nanocavity modes, respectively. κ_1 is the coupling coefficient between the SPPs in the plasmonic waveguide and the vertical nanocavity mode, and κ_2 is the coupling coefficient between the vertical and horizontal nanocavity modes.

To further confirm the all-optical tunability, we subsequently measured the transmission changes (Fig. 3(c)) of the 780-nm signal laser as a function of the incident power. The wavelength of 780 nm located at the center of the transparency window. When the incident power increased from 60 to 90 μW, the transmission of the 780-nm incident light maintained the value of 75%. When the incident power was larger than 97 μW, the transmission of the 780-nm incident light decreased. The reason lies in the fact that the two SPPs absorption induced polymerization of SU-8 caused the redshift of the central wavelength of the transparency window. When the incident power increased to 150 μW, the transmission of the 780-nm incident light decreased to 55%. When the incident power was larger than 150 μW, the transmission of the 780-nm incident light maintained the value of 55%. The reason lies in the fact that all the SU-8 molecules covering the plasmonic nanocavities were polymerized through two SPPs absorption, and the further increment in the incident power could not influence the refractive index of SU-8. We calculated the linear transmission spectrum (Fig. 3(d)) of the plasmonic waveguide side-coupled two plasmonic nanocavities having the SU-8 cover layer with different incident power of 780-nm light by using the finite element method. When the incident power increased from 60 to 150 μW, the central wavelength of the transparency window changed from 780 to 794 nm, i.e., a 14 nm shift in the long wavelength direction was obtained. Accordingly, the transmission of the 780-nm light decreased from 75% (at the incident power of 60 μW) to 55% (at the incident power of 150 μW). This indicates that the central wavelength of the transparency window can be continuously tuned in a range of 24 nm by using two SPPs absorption induced polymerization of SU-8 photoresist.

In summary, we experimentally realized all-optical tunable on-chip PIT in integrated plasmonic circuits based on two SPPs absorption induced polymerization of SU-8 photoresist. A continuous shift range of 24 nm in the transparency window center was obtained. The threshold power of the two SPPs absorption induced polymerization of SU-8 was as low as 100 μW. This not only provides a superior platform for realization of integrated photonic circuits and chips but also offers an efficient approach for the post-processing of

plasmonic microstructures, making up the inadequacy of the microfabrication technology.

This work was supported by the 973 Program of China under Grant Nos. 2013CB328704 and 2014CB921003, the National Natural Science Foundation of China under Grant Nos. 11225417, 61475003, 11134001, 11121091, and 90921008.

[1]G. C. Dyer, G. R. Aizin, S. J. Allen, A. D. Grine, D. Bethke, J. L. Reno, and E. A. Shaner, Nat. Photonics **7**, 925 (2013).
[2]B. Lukyanchuk, N. I. Zheludev, S. A. Maier, N. J. Halas, P. Nordlander, H. Giessen, and C. T. Chong, Nat. Mater. **9**, 707 (2010).
[3]S. Biswas, J. Duan, D. Nepal, K. Park, R. Pachter, and R. A. Vaia, Nano Lett. **13**, 6287 (2013).
[4]C. C. Lu, X. Y. Hu, K. B. Shi, Q. Hu, R. Zhu, H. Yang, and Q. H. Gong, Light: Sci. Appl. **4**, e302 (2015).
[5]P. Tassin, L. Zhang, R. K. Zhao, A. Jain, T. Koschny, and C. M. Soukoulis, Phys. Rev. Lett. **109**, 187401 (2012).
[6]N. Liu, M. Hentschel, T. Weiss, A. P. Alivisatos, and H. Giessen, Science **332**, 1407 (2011).
[7]P. K. Jha, M. Mrejen, J. Kim, C. Wu, X. B. Yin, Y. Wang, and X. Zhang, Appl. Phys. Lett. **105**, 111109 (2014).
[8]A. Artar, A. A. Yanik, and H. Altug, Nano Lett. **11**, 3694 (2011).
[9]F. V. Cube, S. Irsen, R. Diehl, J. Niegemann, K. Busch, and S. Linden, Nano Lett. **13**, 703 (2013).
[10]M. Hentschel, T. Weiss, S. Bagheri, and H. Giessen, Nano Lett. **13**, 4428 (2013).
[11]X. P. Zhang, X. M. Ma, F. Dou, P. X. Zhao, and H. M. Liu, Adv. Funct. Mater. **21**, 4219 (2011).
[12]T. Utikal, T. Zentgraf, T. Paul, C. Rockstuhl, F. Lederer, M. Lippitz, and H. Giessen, Phys. Rev. Lett. **106**, 133901 (2011).
[13]Y. L. Li, H. Yan, D. B. Farmer, X. Meng, W. J. Zhu, R. M. Osgood, T. F. Heinz, and P. Avouris, Nano Lett. **14**, 1573 (2014).
[14]Z. Chai, X. Y. Hu, Y. Zhu, S. B. Sun, H. Yang, and Q. H. Gong, Adv. Opt. Mater. **2**, 320 (2014).
[15]R. D. Kekatpure, E. S. Barnard, W. S. Cai, and M. L. Brongersma, Phys. Rev. Lett. **104**, 243902 (2010).
[16]Y. Zhu, X. Y. Hu, H. Yang, and Q. H. Gong, Sci. Rep. **4**, 3752 (2014).
[17]Z. H. Han and S. I. Bozhevolnyi, Opt. Express **19**, 3251 (2011).
[18]Y. Huang, C. J. Min, and G. Veronis, Appl. Phys. Lett. **99**, 143117 (2011).
[19]C. Kurter, P. Tassin, L. Zhang, T. Komas, A. P. Zhuravel, A. V. Ustinov, S. M. Anlage, and C. M. Soukoulis, Phys. Rev. Lett. **107**, 043901 (2011).
[20]P. Tassin, L. Zhang, T. Komas, E. N. Economou, and C. M. Soukoulis, Phys. Rev. Lett. **102**, 053901 (2009).
[21]N. Papasimakis, V. A. Fedotov, N. I. Zheludev, and S. L. Prosvirnin, Phys. Rev. Lett. **101**, 253903 (2008).
[22]Y. X. Li, F. Liu, L. Xiao, K. Y. Cui, X. Feng, W. Zhang, and Y. D. Huang, Appl. Phys. Lett. **102**, 063113 (2013).
[23]Y. X. Li, F. Liu, Y. Ye, W. S. Meng, K. Y. Cui, X. Feng, W. Zhang, and Y. D. Huang, Appl. Phys. Lett. **104**, 081115 (2014).
[24]M. Deubel, M. Wegener, S. Linden, and G. V. Treymann, Appl. Phys. Lett. **87**, 221104 (2005).
[25]D. Shir, E. C. Nelson, Y. C. Chen, A. Brzezinski, H. Liao, P. V. Braun, P. Wiltzius, K. H. A. Bogart, and J. A. Rogers, Appl. Phys. Lett. **94**, 011101 (2009).
[26]B. H. Cumpston, S. P. Ananthavel, S. Barlow, D. L. Dyer, J. E. Ehrlich, L. L. Erskine, A. A. Heikal, S. M. Kuebler, I. Y. S. Lee, D. McCord-Maughon, J. Qin, H. Rockel, M. Rumi, X. L. Wu, S. R. Marder, and J. W. Perry, Nature **398**, 51 (1999).
[27]M. Thiel, M. S. Rill, G. V. Freymann, and M. Wegener, Adv. Mater. **21**, 4680 (2009).
[28]P. Berini and I. D. Leon, Nat. Photonics **6**, 16 (2012).
[29]A. Archambault, F. Marquier, J. J. Geffet, and C. Arnold, Phys. Rev. B **82**, 035411 (2010).
[30]X. Piao, S. Yu, and N. Park, Opt. Express **20**, 18994 (2012).